Modal Analysis for the Connoisseur

Ron Potter and Norm Olsen, Hewlett-Packard Co., Everett, Washington

A practical model for the transfer matrix of a linear system must include representations of repeated poles (different modes having identical pole values), multiple poles (poles with multiplicity greater than unity), and non-symmetric impedance matrices (generally resulting from rotating components). This article describes measurements of all three of these properties on a very simple mechanical structure.

There was a time when the results of a modal test comprised a tabulation of measured amplitudes for each modal vector, along with an estimate of the resonant frequency of each mode. Later, it became fashionable to display these mode shapes in animated form, and some attempts were made to estimate the damping coefficient of each mode. The early "Normal Mode" concept gave way to the view of conjugate pairs of complex modes.

The ability to visualize modes of vibration is certainly helpful (and often fascinating), but the ultimate goal has always been an estimate of the transfer matrix for the structure, so that the motion for any arbitrary excitation vector could be accurately predicted. It is not enough to have a qualitative "feel" for the shape and frequency of each mode of vibration. Computer models of the structure are needed to optimize the design and to interface with models of other structures.

There are many potential sources of error in estimating modal parameters of some physical systems. Numerous authors have discussed the effects of aliasing, leakage, noise, distortion, etc., and have studied various techniques to minimize errors from these effects. However, there are several basic assumptions upon which elementary modal theory is based that can easily be violated, and may introduce even larger errors than those mentioned.

The following three enhancements need to be appended to elementary modal theory before accurate transfer matrices can be measured:

a. repeated poles
b. cascaded multiple poles
c. non-symmetric transfer matrices.

These enhancements will be discussed individually, and then a very simple example will be given of a structure that can exhibit all three characteristics. This structure has been built and tested, and the test results will be reviewed.

For reference to the theory and notation used in this article, refer to Ref. [1]. Some of the basic equations will be repeated here, for convenience.

Review of Basic Modal Theory

This theory is for linear systems, and the Laplace transforms of all quantities are assumed to exist. The theory will be developed in the Laplace domain, although the inverse transform can be used at any point to obtain an equivalent time function.

Any linear mechanical system (including rotating components) can be described by the equation

$$\mathbf{B(s)X(s)} = \mathbf{F(s)} \tag{1}$$

where, $\mathbf{F}$ is a vector of applied forces, $\mathbf{X}$ is the resulting vector of displacements, and $\mathbf{B}$ is a matrix describing the system, comprising mass, stiffness, and damping matrices in the form of a matrix polynomial in $\mathbf{s}$. The inverse of Eq. (1) is:

$$\mathbf{H(s)F(s)} = \mathbf{X(s)} \tag{2}$$

where,

$$\mathbf{H(s)} = \left[\mathbf{B(s)}\right]^{-1} \tag{2a}$$

is the transfer matrix for the system. This matrix allows the calculation of the displacement vector $\mathbf{X}$ for any applied force vector $\mathbf{F}$. For rotating components, replace force by torque, and linear displacement by angular displacement.

Each element of $\mathbf{H(s)}$ is a rational fraction in the Laplace variable s, and hence can be expressed in partial fraction form as,

$$\mathbf{H(s)} = \sum_{k=1}^{m} \sum_{v=1}^{p_k} \frac{\mathbf{a}_{kv}}{\left(\mathbf{s} - \mathbf{s}_k\right)^v} \tag{3}$$

Here, $\mathbf{k}$ is the index of pole locations, and $\mathbf{v}$ is the index of multiplicity. $\mathbf{a}_{kv}$ is the residue matrix associated with each term in the expansion.

In elementary modal theory, all $\mathbf{p}_k$ are assumed to be unity, and $\mathbf{a}_{kv}$ is assumed to be a symmetric matrix of rank one.

Equation (3) can be written in matrix form as,

$$\mathbf{H(s)} = \mathbf{\Theta\Lambda^{-1}(s)\Psi} \tag{4}$$

where, all $\mathbf{s}$ dependence resides in a quasi-diagonal matrix

$\Lambda^{-1}(\mathbf{s})$. The columns of Θ are the modal vectors, and the rows of Ψ are the transposed bimodal vectors of the system, for a symmetric system, $\Psi = \Theta^{\mathbf{t}}$.

To illustrate the distinction between repeated poles and cascaded multiple poles, along with the effects of a nonsymmetrical system, an example of **H(s)** for 4 modes will be given next. There are two repeated poles, and a pole of multiplicity two. The transfer matrix can be written as:

$$\mathbf{H(s)} =$$
$$\begin{bmatrix} \Theta_1 \Theta_2 \Theta_3 \Theta_4 \end{bmatrix}$$
$$\begin{bmatrix} 0 & (s-a)^{-1} & 0 & 0 \\ (s-a)^{-1} & (s-a)^{-2} & 0 & 0 \\ 0 & 0 & (s-b)^{-1} & 0 \\ 0 & 0 & 0 & (s-b)^{-1} \end{bmatrix} \begin{bmatrix} \Psi_1 \\ \Psi_2 \\ \Psi_3 \\ \Psi_4 \end{bmatrix}$$

$$(5)$$

Here, Θ_k are the columns of Θ (modal vectors) and Ψ_k are the rows of Ψ (transposed bimodal vectors). The multiple pole is at $\mathbf{s} = \mathbf{a}$, and the repeated poles are at $\mathbf{s} = \mathbf{b}$. Notice the triangular form of the sub-matrix of $\Lambda^{-1}(\mathbf{s})$ that is associated with the multiple pole. The inverse of this sub-matrix is a version of the Jordan normal form of a matrix whose determinant has a multiple zero. For example:

$$\Lambda(\mathbf{s}) = \begin{bmatrix} -1 & (s-a) & 0 & 0 \\ (s-a) & 0 & 0 & 0 \\ 0 & 0 & (s-b) & 0 \\ 0 & 0 & 0 & (s-b) \end{bmatrix}$$

$$(6)$$

There are several equivalent ways to express this triangular form, by rotating the triangle, or by changing signs on elements. The form indicated in Equations (5) and (6) has been chosen to preserve some degree of symmetry between the modal and bimodal vectors. If **H(s)** is written in expanded form, the result is:

$$\mathbf{H(s)} = \frac{\Theta_1 \Psi_2 + \Theta_2 \Psi_1}{s-a} + \frac{\Theta_2 \Psi_2}{(s-a)^2} + \frac{\Theta_3 \Psi_3 + \Theta_4 \Theta_4}{s-b}$$

$$(7)$$

The first two elements of Θ and Ψ appear in cross-product form as the residue matrix for the first order pole at $\mathbf{s} = \mathbf{a}$, while only the second elements are used for the second order pole at $\mathbf{s} = \mathbf{a}$. This is a convenient arrangement, especially for

higher order multiplicities. Equations (5) or (7) will be used to illustrate the three concepts that form the theme of this article.

Repeated Poles. Repeated poles are those with the same numerical value that are associated with different modal vectors. Any linear combination of such modal vectors is also a valid modal vector, so it is always possible to find a set of mutually orthogonal modal vectors that span the sub-space associated with a given pole value and order.

The term "repeated" pole connotes the possibility of expressing the partial fraction expansion of the transfer function as the sum of terms having identical poles and multiplicities, but different residues. The same pole appears repeatedly in the expansion.

Repeated poles are bound to occur in structures having some degree of spatial symmetry. This includes circles, squares, regular polygons, cylinders based on these shapes, and more symmetrical objects such as spheres. In addition, there are nonsymmetrical shapes that can have repeated poles, somewhat by chance. For example, imagine two structures that happen to have the same pole value, but are interconnected at nodal points of their respective mode shapes. If the mutual coupling is sufficiently small, the poles will be nearly identical, and a repeated pole model will be valid for all practical purposes.

If a structure having repeated poles is excited, the resulting response will comprise some (unknown) linear combination of all modes in the group. Any transfer matrix model based upon a single mode will not predict the correct response if some other excitation vector is chosen, since some new (but still unknown) linear combination of modal vectors will result. Thus, any transfer matrix model that ignores repeated modes is doomed to failure if such modes exist in the frequency range of interest.

The rank of the residue matrix for a repeated pole is equal to the number of different modes. The last term in Eq. (7) shows an example of two repeated poles at $\mathbf{s} = \mathbf{b}$. Note the rank two residue matrix.

Multiple Poles. When the modal vectors associated with repeated poles become lightly coupled (meaning that pole values remain essentially unchanged), the possibility arises that the motion of one mode might act as a driving excitation for another mode. The resulting transfer function is a cascade of two simple poles, which is a pole of multiplicity two.

Technically, coupled modes cannot have identical pole values, but practically it may be necessary to use the multiple pole model. The reason is that the modal vectors associated with a pair of simple poles become nearly co-linear when the pole values are similar. The representation of any vector in a direction orthogonal to either one of the pair will be very poor, and very sensitive to any errors in the data or in computer calculations. At some point, as two pole values converge, it is necessary to

switch from the single pole form to the multiple pole form, simply to preserve accuracy in the transfer matrix model.

When an $\mathbf{n}^{\text{th}}$ order multiple pole is found, there will also be poles having all lower multiplicity values, as well. For example, in Eq. (7), the 2nd term is the 2nd order pole at $\mathbf{s} = \mathbf{a}$, and the 1st term gives the contribution of a first order pole at $\mathbf{s} = \mathbf{a}$. Note that the rank of the residue matrix of the 1st term is two, while that for the second term is only unity (the term "residue" is used here to represent the numerator of any multiplicity pole, and not just that of a simple pole). Also, note that only two modal vectors are used for both terms, and that they are combined in a specific manner. This is insured by, the form of the $\mathbf{\Lambda^{-1}(s)}$ matrix illustrated in Eq. (5). The sum of the rank of the numerator and the multiplicity of the denominator is a constant for a given multiple pole.

Multiple poles can only be identified, by inspecting the measured set of transfer functions. The shape of the multiple pole transfer characteristic is somewhat different than that of a simple pole. For example, there is a phase shift of $\mathbf{n \times 180°}$ as an $\mathbf{n}^{\text{th}}$ order pole is passed along the frequency axis. The roll-off rate is also faster for higher order poles. In most measuring systems, it is the job of the curve fitter and root solver to identify multiple poles, and to determine the residue matrix elements for each pole of lower order (via the conversion from a rational fraction form to a partial fraction form, for example).

In contrast to the case for repeated poles, it is not necessary to measure extra rows or columns of a multiple pole to determine the set of modal vectors, even though the rank of some residue matrices might be greater than unity. This is because of the required cross-structure between terms of a multiple pole model. For example, in Eq. (7), the vectors $\mathbf{\Theta_2}$ and $\mathbf{\Psi_2^t}$ can be obtained from the residue of the 2nd term alone. Then, given those two vectors, the residue of the first term can be used to calculate $\mathbf{\Theta_1}$ and $\mathbf{\Psi_1}$.

However, as was true for repeated poles, it is always possible to find an orthogonal set of modal vectors for a multiple pole. The number of options is more restricted for the multiple pole than for a repeated pole, due to the built-in cross-structure.

Whenever repeated poles exist, there is a good chance that a multiple pole can be found. When "symmetric" structures are slightly asymmetric, some small amount of coupling between modes is likely. Another small-coupling mechanism can be caused by a large impedance mismatch, as illustrated by the antenna on top of a battleship, where both structures share one pole value in common. If the battleship is excited at this frequency, the transfer function to the tip of the antenna will comprise a pole of multiplicity two.

Even though repeated poles and multiple poles may coexist in a structure (at the same pole value), they are different concepts and enter into the transfer matrix model in different ways. They are also calculated from measured transfer functions in different ways. The representation of mode shapes of multiple poles is more sensitive to measurement errors than is the representation of repeated poles, but the consequences of an erroneous transfer matrix model are probably greater in the repeated pole case than for the multiple pole case.

Non-symmetric Matrices. Equation (7) illustrates the form of a transfer matrix that is not symmetric. The modal vectors (columns of $\mathbf{\Theta}$) are not the same as the bimodal vectors (columns of $\mathbf{\Psi^t}$) unless the system is symmetric. This implies that both rows and columns must be measured for each mode. All points on the structure must be excited to measure a row, and the motion of all points must be measured to determine a column. For a residue matrix of rank $\mathbf{r}$, it is necessary to measure $\mathbf{r}$ rows and $\mathbf{r}$ columns.

Since the equations for a pure gyroscope are anti-symmetric (see Appendix), it follows that any transfer matrix that is significantly influenced by rotating components will be non-symmetric. This obviously includes a large proportion of the various structures of interest, so non-symmetric transfer matrices are difficult to avoid, in practice. As can be seen from Eq. (7), a non-symmetric transfer matrix based upon a symmetric model is simply not correct, and may be of little value in predicting system behavior.

A Physical Example

Figures 1 and 2 show a very simple structure that can have repeated poles, multiple poles, and a non-symmetric transfer matrix. The weights on the horizontal bar can be positioned anywhere along the bar outboard of the vertical springs. This configuration allows for the torsion mode about the $\mathbf{y}$-axis to be tuned to have its resonant frequency below, above or the same as the resonant frequency of the bending mode in the $\mathbf{z}$-direction. At the center of the horizontal bar a rotating element consisting of an instrument cooling fan was attached with its axis of rotation in the $\mathbf{z}$-direction. With the rotating element stationary, the structure was tuned so that the torsion and bending modes had the same pole value. This produces a pair of repeated modes.

For a small value of angular momentum $\mathbf{H_z}$ in the z-direction, the gyroscopic effect introduces a small amount of coupling between the two modes. If the bending mode is excited, the rotating component will, in turn, excite the torsional mode. The resulting composite transfer function between bending mode excitation and torsional mode motion will exhibit a second order pole. However, as indicated in Eq. (7), it is possible that both first and second order poles will occur, so some care is needed to avoid direct excitation of the first order component. This will allow the second order contribution to be seen more clearly.
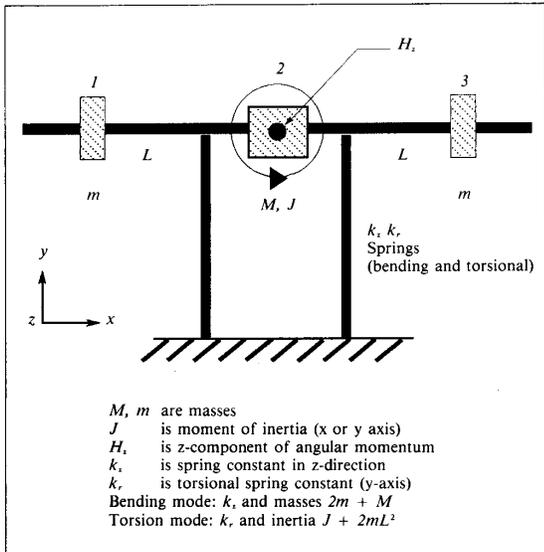
Figure 1. Component diagram of test system.

M, m are masses
J is moment of inertia (x or y axis)
H_z is z-component of angular momentum
k_z is spring constant in z-direction
k_r is torsional spring constant (y-axis)
Bending mode: k_z and masses $2m + M$
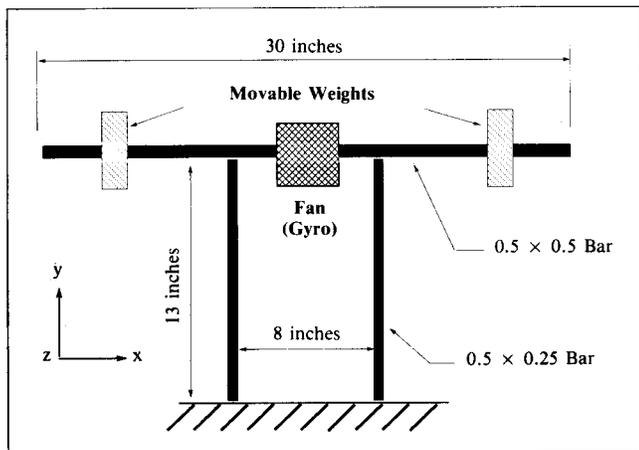Torsion mode: k_r and inertia $J + 2mL^2$

Figure 2. Dimensional diagram of test system.

Since the rotating component has an anti-symmetric transfer characteristic (see Appendix), the entire structure will exhibit a non-symmetric transfer matrix, as long as the rotation is sufficiently rapid. For example, assume a positive excitation in the **z**-direction at node 2. This will eventually cause a positive angular rotation around the **y**-axis. In contrast, a positive torque applied about the **y**-axis will produce a bending motion in the negative **z**-direction.
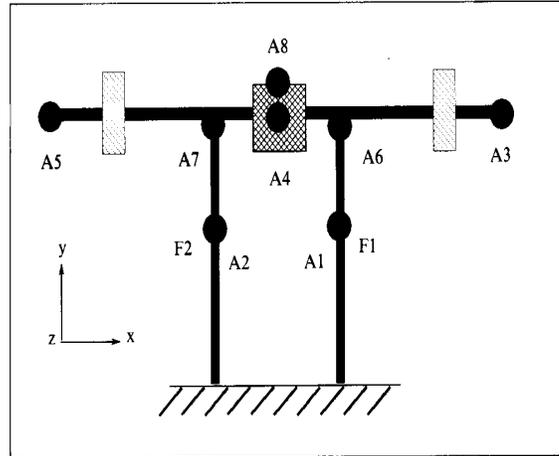
Figure 3. Transducer locations.
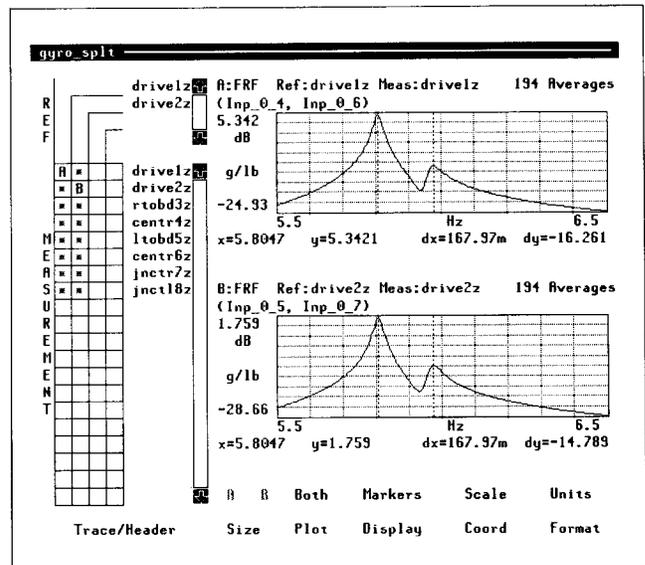
Figure 4. Modes separated case: upper trace - driving point magnitude, location #1; lower trace – driving point magnitude, location #2.

Once the basic structure was assembled, the shakers were attached through stingers to force transducers at force locations F1 and F2. A total of eight accelerometers were used; one at each driving point location and the remaining six along the horizontal bar (Figure 3).

The gyro was simply an instrument cooling fan, which had a cast rotor construction with many blades. This device exhibited a reasonable gyroscopic effect for its size and weight. It remained attached to the structure during all the measurements.
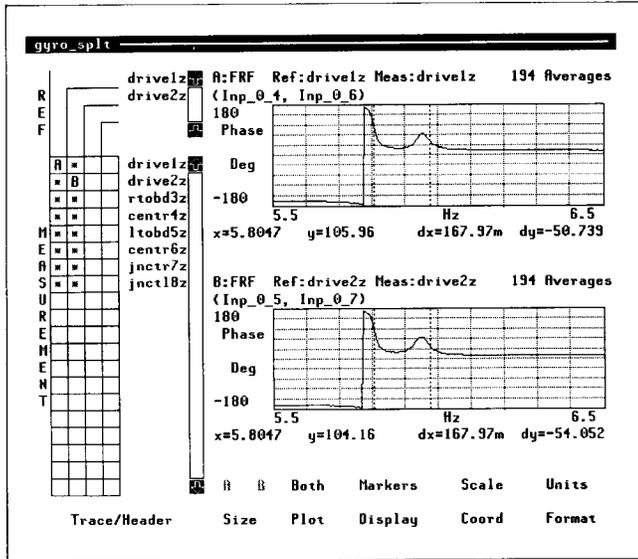
Figure 5. Modes separated case: upper trace - driving point phase, location #1; lower trace - driving point phase, location #2.
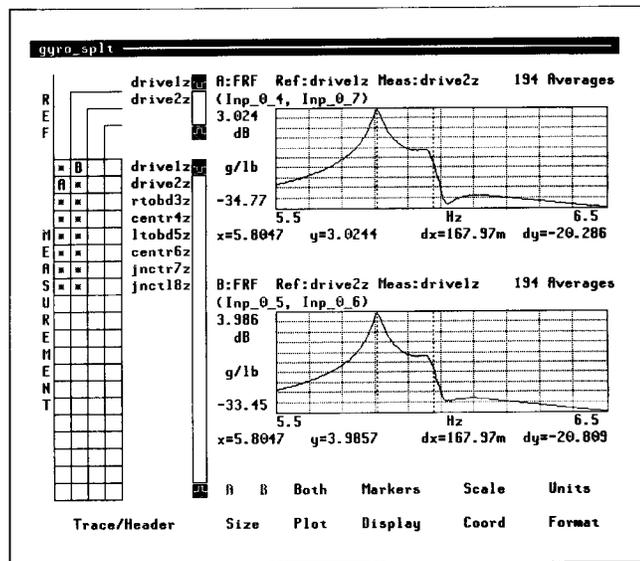

Figure 6. Modes separated case: reciprocity comparison – magnitude, location 2/1 versus 1/2.

The first set of measurements was made with the movable masses adjusted to an inboard position setting up the case where the first bending mode is lower in frequency than the first torsion. The gyro was not operating during this measurement sequence.

The HP3565S multiple channel dynamic signal analysis system was used to make the measurements. All 16 frequency response functions were measured simultaneously using this system hardware and the HP VISTA signal processing software. This system provides the capability of performing the

Multiple-Input Multiple-Output frequency response measurements using an algorithm that is an outgrowth of that discussed in References [2, 3, 4, and 5]. These frequency response measurements were made using uncorrelated burst random excitations on each shaker.

Modes Well Separated. Figure 4 shows the two driving point frequency response functions with the cursors set to the approximate resonant frequencies of 5.8 and 5.97 Hz. The upper plot (trace A) is the frequency response at driving point location 1 (the response at location 1 due to the force at location 1). The association between measurement and trace is shown via the matrix on the left side of the plot; with trace A always being the upper trace. The phase plots for the two driving points are shown in Figure 5.

The next plot, Figure 6, shows the cross measurement between the two driving point locations, corresponding to the response at point 2 due to the force at point 1 and the response at point I due to the force at point 2. These two plots should be identical since reciprocity should be valid for this simple system. The corresponding phase plot is shown in Figure 7. The agreement is fairly good except for an absolute gain error caused by the low frequency characteristics of the transducers used. The transducer sensitivities measured at 100 Hz were used with the assumption that there were no gain or phase differences of significance in the measurement frequency range. As later verified, this assumption was incorrect. This first measurement configuration was primarily a reference to obtain confidence that the setup was correct and good measurements were possible. Curve fitting these results was straightforward and produced frequencies of 5.806 and 5.966 Hz and damping factors of 0.196% and 0.364% respectively for the torsion and bending modes.

Repeated Mode Case. The next set of measurements was made after the movable weights were repositioned to obtain the repeated pole case. Figure 8 shows the magnitude of the driving point measurements, and Figure 9 the phase plots (Trace A = 1/1 and Trace B = 2/2). Figures 10 and 11 present the cross measurements between the two driving point locations (Trace A = 2/1 and Trace B = 1/ 2). Again, except for the 1 dB absolute gain error, the reciprocity check of these two measurements is very good in both magnitude and phase.

As is typical of modal data that contains repeated poles (or modes), there is nothing obvious in the plotted data that makes this fact stand out. In just looking at the data, it appears to be what one would see if there were but a single mode in this frequency range. If the data were obtained with only a single shaker location there would be no method to determine that a repeated pole existed in this frequency range. This data set was obtained with two shaker locations, and by using techniques like Polyreference , the detection and characterization of a repeated pole can be accomplished. The detection and characterization of a repeated pole can be accomplished.
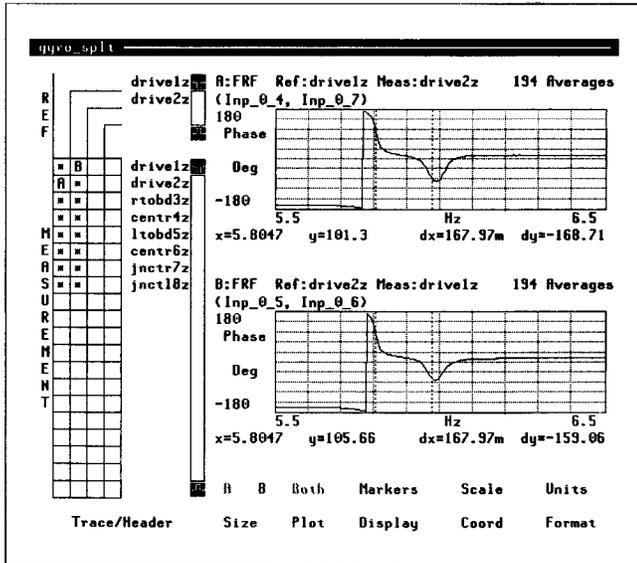
Figure 7. Modes separated case: reciprocity comparison – phase, location 2/1 versus 1/2.
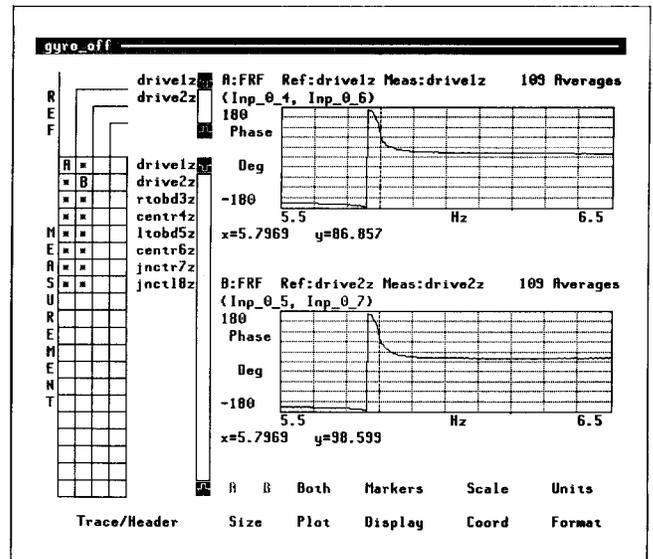

Figure 9. Repeated mode case: upper trace - driving point phase, location #1; lower trace - driving point phase, location #2.
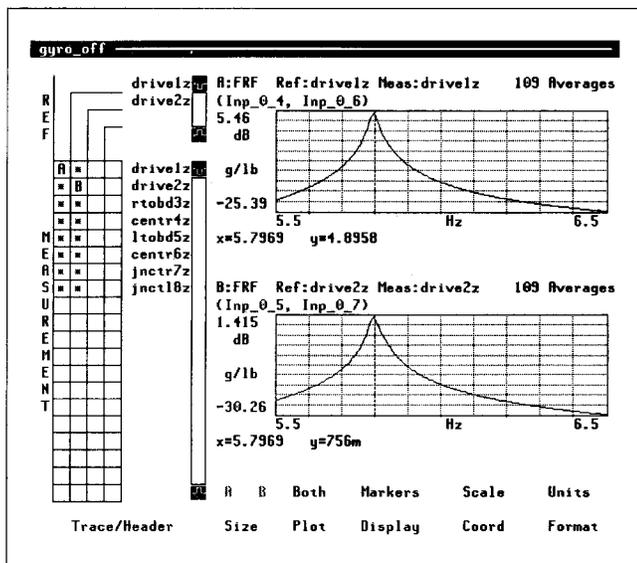

Figure 8. Repeated mode case: upper trace - driving point magnitude, location #1; lower trace - driving point magnitude, location #2.
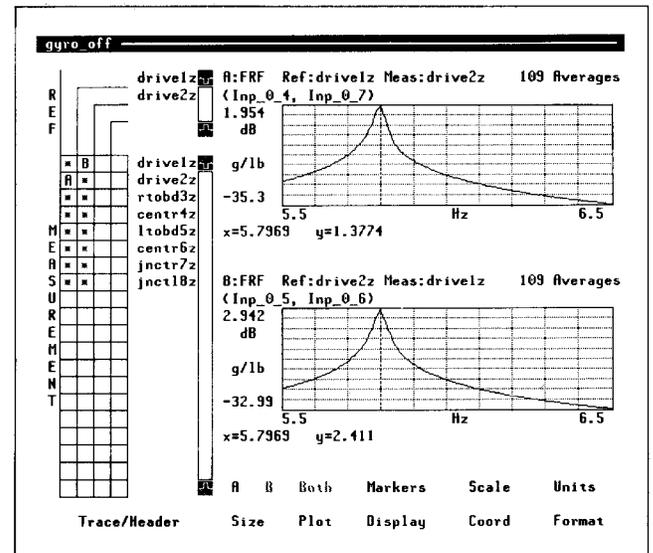

Figure 10. Repeated mode case: reciprocity comparison – magnitude, location 2/1 versus 1/2.

Using such a technique with this data set produced two modes with frequencies of 5.793 and 5.816Hz with damping factors of 0.207% and 0.389% respectively.

Non-symmetric Case. The physical configuration for this third set of measurements is identical to that for the repeated pole case, with the exception that the fan (gyro) was turned on and was allowed to run at its normal speed. One effect of the gyro is to couple the two modes. Figure 12 shows the two driving point measurements in magnitude form. Note that one observable effect of the gyro is to split the repeated pole into two

distinct resonant peaks. Figure 13 shows the phase plots of these driving point measurements.

Comparing the cross measurements between the two driving points (Trace A = 2/1 and Trace B = 1/2) in Figure 14 reveals that this measurement fails the reciprocity relationship of a symmetric system (where these two measurements would look identical). The corresponding phase plots in Figure 15 also reveal different characteristics.
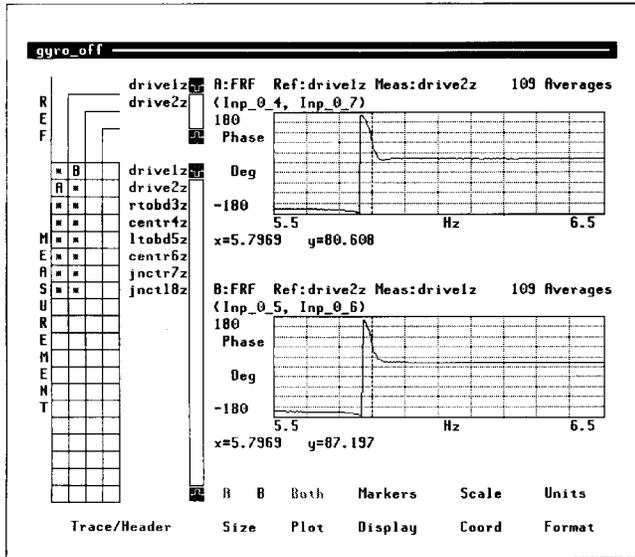
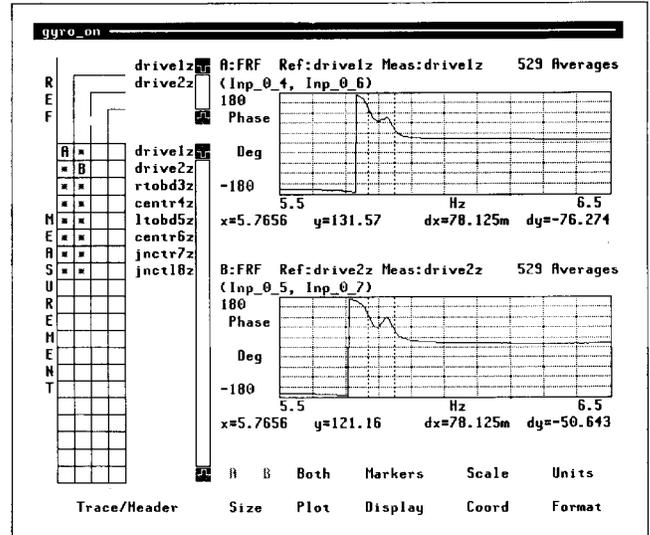*Figure 11. Repeated mode case: reciprocity comparison – phase, location 2/1 versus 1/2.*

Figure 13. Gyro effects on repeated mode case: upper trace - driving point phase, location #1; lower trace - driving point phase, location #2.
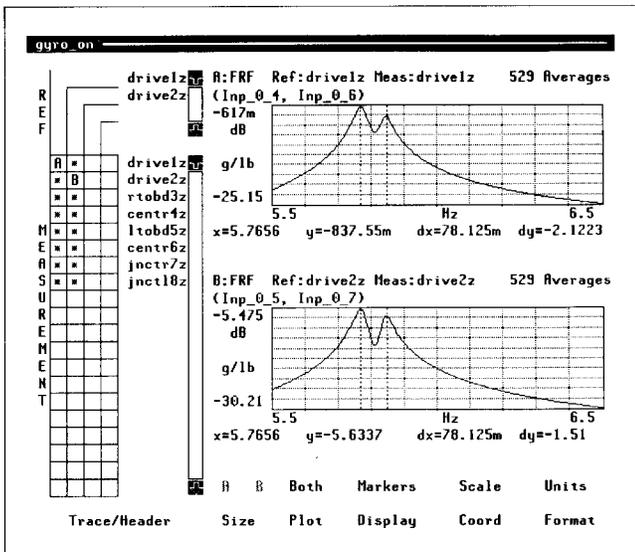

Figure 12. Gyro effects on repeated mode case: upper trace – driving point magnitude, location #1; lower trace – driving point magnitude, location #2.
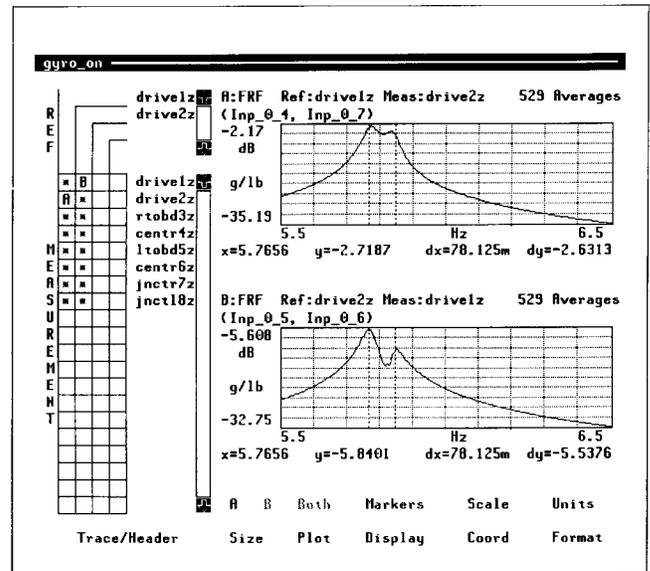

Figure 14. Gyro effects on repeated mode case: reciprocity comparison magnitude, location 2/1 versus 1/2.

In this system, it is no longer sufficient to measure one row or column of the frequency response matrix to estimate the entire matrix. One would need to measure both rows and columns to completely characterize the system.

Multiple Poles. In the last example, the structure of the preceding examples was simplified by removing the horizontal bar, along with the weights and fan, leaving just the two vertical springs "isolated" from each other. This was done to eliminate any coupling via a unit multiplicity pole term in the transfer function between input force and output response. An effort was

then made to tune each of these "separate" cantilevered beams to have the same frequency and damping.

Having come reasonably close to achieving this, a frequency response measurement was made with the force at point 1 on one of the cantilevered beams and the response at point 2 on the other cantilevered beam. The only coupling between these two cantilevered beams is through the 2 inch thick aluminum base to which the beams are attached. This coupling is small, in that very little motion is seen on the second beam when exciting the first. The response of the second beam is due to a cascading or
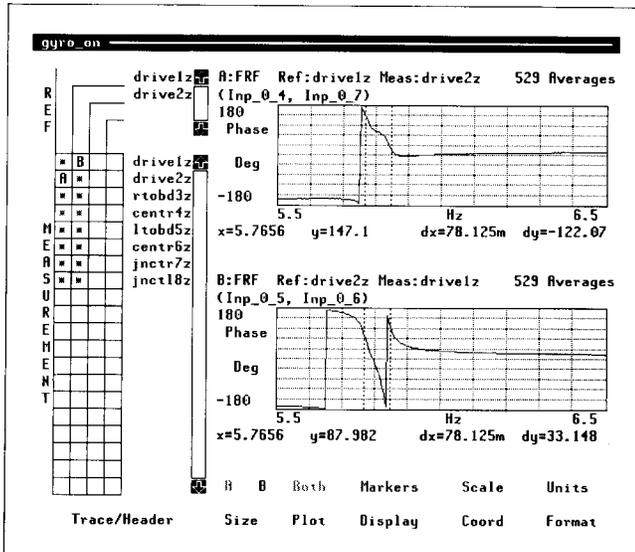
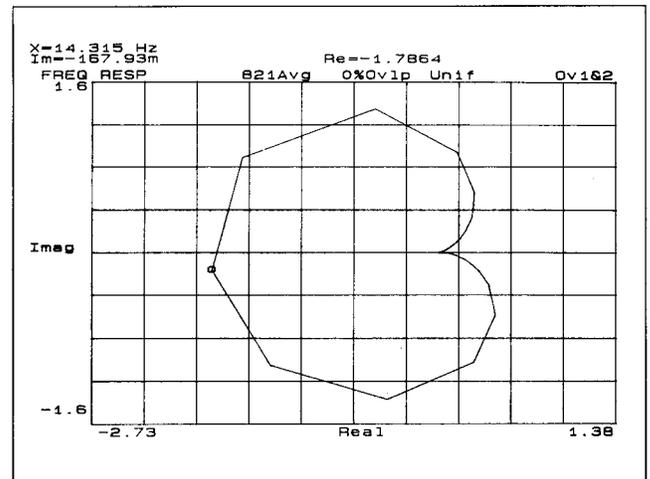*Figure 15. Gyro effects on repeated mode case: reciprocity comparison phase, location 2/1 versus 1/2.*
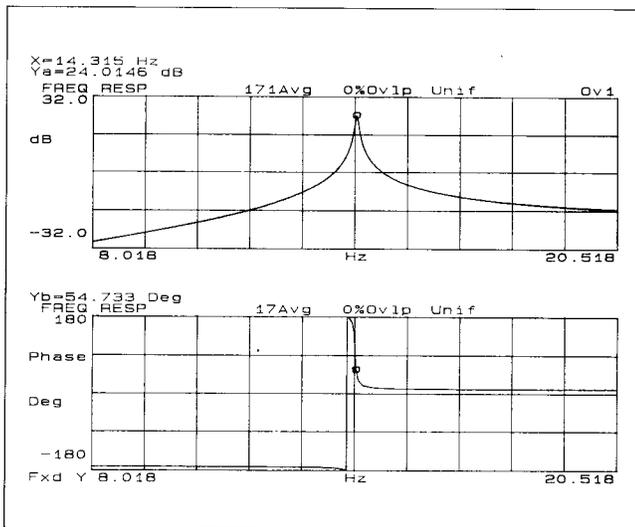

Figure 16. Response of Beam 2 due to force at Beam 1.

Figure 17 Complex plane plot of response of Beam 2 due to force at Beam 1.

Figure 18. Driving point measurement of Beam 2.

multiplication of the two individual modes. After averaging many burst random excitations (821), a reasonable frequency response function was obtained.

Figure 16 shows the magnitude and phase of this frequency response function measurement. Note the 180° phase swing characteristic of the resonance. Figure 17 shows the complex plane or Nyquist format of the same measurement. For reference, Figure 18 is the driving point frequency response of the second beam by itself that was obtained during the tuning phase. These measurements were obtained with the HP3562A, two-channel dynamic signal analyzer. The curve fitter in the HP3562A was used on the measurement of Figure 16 in an automatic mode. Within some user specified upper limit on the
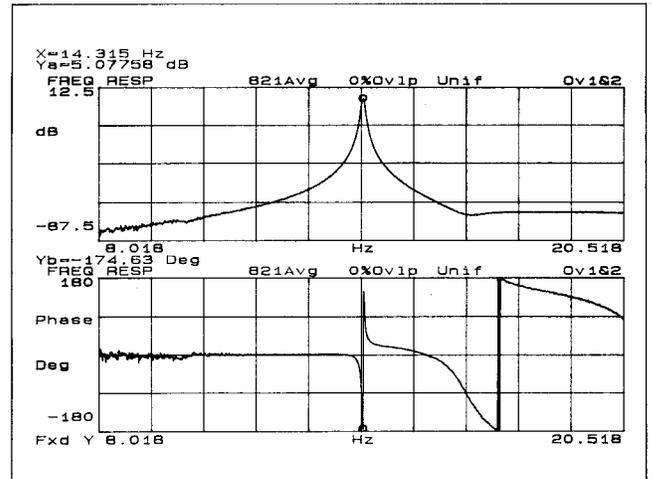
number of poles and zeros, this curve fitter will use both the frequency response function and the coherence function to determine both the number and values of the poles and zeros in the measurements.[8] With an upper limit of 10 poles and 10 zeros the table in Figure 19 gives the curve fit results. This shows two poles very close together, but not a pole of multiplicity of 2. If the form of these, pole/zero curve fit results are converted to pole/residue form the results are shown in Figure 20.

From a modal analysis point of view the pole/residue form is needed in order to determine the mode shape. Note that, the two residues are almost exactly opposite in sign to each other. As the two poles get closer and closer together these two residues will get larger, with opposite sign but nearly the same magnitude. Because of numerical problems, at some point it would be better to use a multiple pole formulation instead of two almost identical single poles.
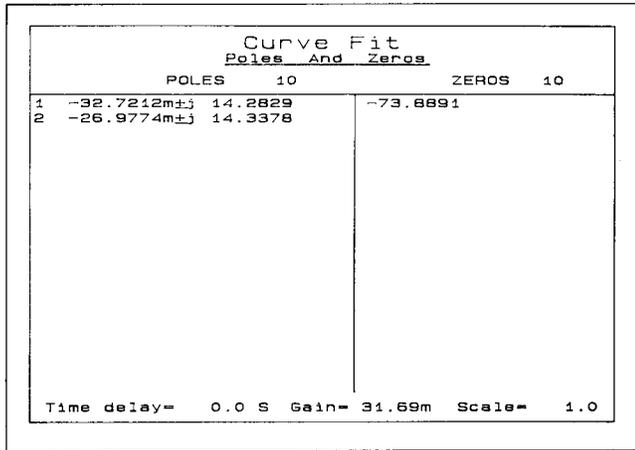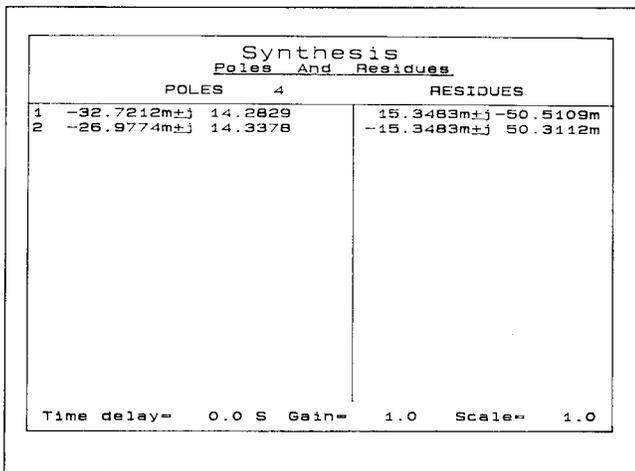
Figure 19. Curve fit of Figure 16 data.

Figure 20. Conversion of pole/zero form of Figure 19 to pole/residue form.

If the "equivalent" multiple pole is chosen as the arithmetic mean between the two poles in Figure 20, then the residues for the first order part are $\pm\, j1.9967 \times 10^{-4}$ and the residues for the second order part are $-28.5737 \times 10^{-4} \pm j5.5362 \times 10^{-4}$.

Summary and Conclusions

Any practical model for a transfer matrix of a linear system must have the capability to represent repeated poles, multiple poles, and non-symmetric system impedance elements. All three of these characteristics are likely to occur in many structures of interest, and in those cases, the transfer matrix model will be of little value without these features

As an illustration of these concepts, a very simple mechanical structure is shown that includes all three characteristics. This structure has been built and tested, and the test results are included in this article. The simplicity of this structure probably implies that these properties are relatively common in more complicated structures.

It should also be apparent that all transducers must be carefully calibrated at all frequencies, in order to obtain the correct modal vector components. A complete set of calibration data should be obtained before and after the test to insure reliable data.

References

1. Potter, R. W., "A General Theory of Modal Analysis for Linear Systems," The Shock and Vibration Digest, Vol. 7, No. 11, November 1975, pp 8-11.

2. Allemang, R. J., Rost, R. W., and Brown, D. L., "Multiple Input Estimation of Frequency Response Functions: Excitation Considerations," ASME Paper Number 83-DET-73, 1983, pp 11.

3. Potter, R. W., "Matrix Formulation of Multiple and Partial Coherence," Journal of the Acoustical Society of America, Volume 66, Number 3, March 1977, pp 776-781.

4. Allemang, R. J., "Investigation of Some Multiple Input/Output Frequency Response Function Experimental Modal Analysis Techniques," Doctor of Philosophy Dissertation, University of Cincinnati, Mechanical Engineering Department, 1980, pp 358.

5. Allemang, R. J., Brown, D. L., and Rost, R. W., "Dual Input Estimation of Frequency Response Functions for Experimental Modal Analysis of Automotive Structures," SAE Paper Number 820193.

6. Deblauwe, E and Allemang, R. J., "The Polyreference Time Domain Technique," Proceedings, 5th International Modal Analysis Conference, London, England, 1987.

7. Vold, H. end Rocklin, T., "The Numerical Implementation of a Multi-Input Modal Estimation Algorithm for Mini-Computers," Proceedings, International Modal Analysis Conference, pp 542-548, 1982.

8. Adcock, J. and Potter, R., "A Frequency Domain Curve Fitting Algorithm with Improved Accuracy," International Modal Analysis Conference Proceedings, January 1985, pp 541.

9. Thaler, G. J. and Brown, R. G., "Analysis and Design of Feedback Control Systems," McGraw-Hill, New York, 1960, pp 133-135.

Appendix - Gyroscopic Impedance Matrix

Assume a z-direction spin axis with angular momentum $\mathbf{H}$ (For an inertially symmetrical rotor spinning at a constant speed $\boldsymbol{\omega}_z$, $\mathbf{H} = \mathbf{I}\boldsymbol{\omega}_z$ where $\mathbf{I} =$ moment of inertia about an in plane axis.). Since $\mathbf{H}$ is conserved, an infinitesimal perturbation in angle $\mathbf{d\Theta}$ will cause $\mathbf{dH} = -\mathbf{Hd\Theta}$ perpendicular to $\mathbf{H}$. If this occurs in a time interval $\mathbf{dt}$, then:

$$\mathbf{dH}/\mathbf{dt} = -\mathbf{H}\left(\mathbf{d\Theta}/\mathbf{dt}\right) = -\mathbf{H}\boldsymbol{\omega} = \mathbf{T} \quad \text{(torque equation)}$$

For example, a component of torque applied about the x-axis results in an angular velocity $\boldsymbol{\omega}_y$ about the y-axis. A y-axis torque component results in a negative x-axis angular velocity. Thus: [9]

$$\mathbf{T}_z = \mathbf{H}\boldsymbol{\omega}_y \quad \mathbf{T}_y = -\mathbf{H}\boldsymbol{\omega}_z$$

In matrix form, these equations can be written as:

$$\mathbf{T} = \mathbf{Z}_g\mathbf{W} \text{, where}$$

$$\mathbf{T} = \begin{bmatrix} \mathbf{T}_x \\ \mathbf{T}_y \end{bmatrix}, \quad \mathbf{W} = \begin{bmatrix} \boldsymbol{\omega}_x \\ \boldsymbol{\omega}_y \end{bmatrix}, \quad \mathbf{Z}_g = \begin{bmatrix} 0 & \mathbf{H} \\ -\mathbf{H} & 0 \end{bmatrix}$$

Note that the gyroscopic impedance $\mathbf{Z}_g$ is anti-symmetric. This will eliminate symmetric matrices when significant rotating components are present.

In practice, there are generally both source and load impedances connected to the gyroscope, so the torque equations can be generalized to:

$$\mathbf{T}_x = \mathbf{Z}_x\boldsymbol{\omega}_x + \mathbf{H}\boldsymbol{\omega}_y$$

$$\mathbf{T}_y = \mathbf{Z}_y\boldsymbol{\omega}_y - \mathbf{H}\boldsymbol{\omega}_x \text{, or}$$

$$\mathbf{T} = \mathbf{ZW,} \text{ where}$$

$$\mathbf{Z} = \begin{bmatrix} \mathbf{Z}_x & \mathbf{H} \\ -\mathbf{H} & \mathbf{Z}_y \end{bmatrix}$$

The inverse expression is:

$$\mathbf{W} = \mathbf{Z}^{-1}\mathbf{T} \text{, where}$$

$$\mathbf{Z}^{-1} = \frac{1}{\mathbf{Z}_x\mathbf{Z}_y + \mathbf{H}^2} \begin{bmatrix} \mathbf{Z}_y & -\mathbf{H} \\ \mathbf{H} & \mathbf{Z}_x \end{bmatrix}$$

Assume that the external applied torque is in the x-direction, so that:

$$\mathbf{T}_y = \mathbf{0} \text{, then}$$

$$\boldsymbol{\omega}_x = \frac{\mathbf{Z}_y\mathbf{T}_x}{\mathbf{Z}_x\mathbf{Z}_y + \mathbf{H}^2} \text{, (input angular velocity)}$$

$$\boldsymbol{\omega}_y = \frac{\mathbf{H}\mathbf{T}_x}{\mathbf{Z}_x\mathbf{Z}_y + \mathbf{H}^2} \text{, (output angular velocity)}$$

$$\mathbf{Z}_{in} = \frac{\mathbf{T}_x}{\boldsymbol{\omega}_x} = \mathbf{Z}_x + \frac{\mathbf{H}^2}{\mathbf{Z}_y} \text{, (input impedance)}$$

$$\boldsymbol{\omega}_y/\boldsymbol{\omega}_x = \mathbf{H}/\mathbf{Z}_y \text{, (angular velocity transfer function)}$$

Notice that the gyroscope inverts the load impedance $\mathbf{Z}_y$, and adds a portion of that inverse to the original $\mathbf{Z}_x$. The angular transfer function is also proportional to $1/\mathbf{Z}_y$, and is proportional to the gyroscope angular momentum $\mathbf{H}$, whereas the input impedance transfer function is proportional to $\mathbf{H}^2$.